FULL PAPER

Magnetic Resonance in Medicine 00:00–00 (2016)

Materials and Methods for Higher Performance Screen-Printed Flexible MRI Receive Coils

Joseph R. Corea, P. Balthazar Lechene, Michael Lustig,* and Ana C. Arias*

Purpose: To develop methods for characterizing materials used in screen-printed MRI coils and improve signal-to-noise ratio (SNR) with new lower-loss materials.

Methods: An experimental apparatus was created to characterize dielectric properties of plastic substrates used in receive coils. Coils were fabricated by screen printing conductive ink onto several plastic substrates. Unloaded and sample loaded quality factor ($Q_{Unloaded}/Q_{Loaded}$) measurements and scans on a 3T scanner were used to characterize coil performance. An experimental method was developed to describe the relationship between a coil's $Q_{Unloaded}$ and the SNR it provides in images of a phantom. In addition, 3T scans of a phantom and the head of a volunteer were obtained with a proof-of-concept printed eight-channel array, and the results were compared with a commercial 12-channel array.

Results: Printed coils with optimized substrates exhibited up to 97% of the image SNR when compared with a traditional coil on a loading phantom. $Q_{Unloaded}$ and the SNR of coils were successfully correlated. The printed array resulted in images comparable to the quality given by the commercial array.

Conclusion: Using the proposed methods and materials, the SNR of printed coils approached that of commercial coils while using a new fabrication technique that provided more flexibility and close contact with the patient's body. **Magn Reson Med 000:000–000, 2016. © 2016 International Society for Magnetic Resonance in Medicine**

Key words: MRI coils; flexible MRI coils; phased arrays; NMR probes; screen printing; plastic substrates

INTRODUCTION

In MRI, surface receive coils are placed in close proximity to the patient's body in order to provide images with high signal-to-noise ratio (SNR) (1–3). These coils consist of loops of wire divided by in-series capacitors that form a resonating LC circuit. By varying the value of the capacitors, the coils are tuned to resonate at the Larmor frequency (4–6). Large coils have an increased field of view but yield a lower SNR than smaller coils (7). Therefore, high-density arrays with small elements are desirable for large field of view coverage with improved SNR (1).

There are several sources of loss that can reduce image SNR. Although the materials used in coil fabrication can contribute to these losses, the patient (i.e., the sample) usually contributes the largest portion of total loss in clinical scenarios at 1.5T and 3T (8). A common way to characterize the origin of losses (i.e., the effective resistance) generated by a coil sample system is to measure the coil's quality factor (Q) with and without the presence of conductive (i.e., loading) materials (Q_{Loaded} and $Q_{Unloaded}$, respectively). The losses associated with materials used in the fabrication of coils can be inferred from the value of $Q_{Unloaded}$, whereas Q_{Loaded} provides insight about loss contribution from the sample. Higher Q indicates less loss, which translates into better SNR in images (7).

The current strategy used in conventional coil fabrication is to get the highest possible $Q_{Unloaded}$ by using materials with very low electrical loss such as thick bulk copper traces and high-quality porcelain capacitors (9). This method works well in cases where the sample noise is not the dominant factor, as is the case in low-frequency MR, NMR systems, or preclinical imaging where both the sample and the coils are small. However, in clinical scenarios where the patient is the largest source of loss, as the coil's $Q_{Unloaded}$ continues to increase, only a marginal increase in SNR is observed (8). With a reduced emphasis on the material's electrical properties, unconventional materials and processes, which offer other advantages, can be leveraged without incurring a large SNR penalty. For example, though less conductive than copper foil, conductive traces printed from solution by additive manufacturing techniques such as screen-printing (10) can be used to create electrically active patterns, producing flexible and lightweight coils.

We have shown in prior work that flexible screen-printed coils with relatively low $Q_{Unloaded}$ could generate images within 20% of a high-quality control at the same distance from the sample (11). Furthermore, the high flexibility of printed coils enables them to surpass conventional coils when they fit better and are closer to the sample (11). Printing also represents a quick fabrication pathway, ideal for unique applications, as shown previously by inkjet printing coils on polyimide film for use in small animal systems (12) and a 3D-printed NMR coil (13). In these applications, the sample is usually small, causing less of the total loss to come from the sample. Unlike imaging larger samples found in clinical scanning, this puts more emphasis on the quality of materials

Department of Electrical Engineering and Computer Sciences, University of California, Berkeley, Berkeley, California, USA

Grant sponsor: National Institutes of Health; Grant numbers: R21 EB015628 and R01 EB019241; Grant sponsors: the Hellman Family Fund, Sloan Research Fellowship, an Okawa Research Grant, the Bakar Fellowship, and GE Healthcare.

*Correspondence to: Ana C. Arias, Ph.D., 508 Cory Hall, Berkeley CA, 94720. E-mail: acarias@eecs.berkeley.edu or Michael Lustig, Ph.D., 506 Cory Hall, Berkeley, CA 94720. E-mail: mlustig@eecs.berkeley.edu

Received 27 May 2016; revised 19 July 2016; accepted 9 August 2016
DOI 10.1002/mrm.26399
Published online 00 Month 2016 in Wiley Online Library (wileyonlinelibrary.com).

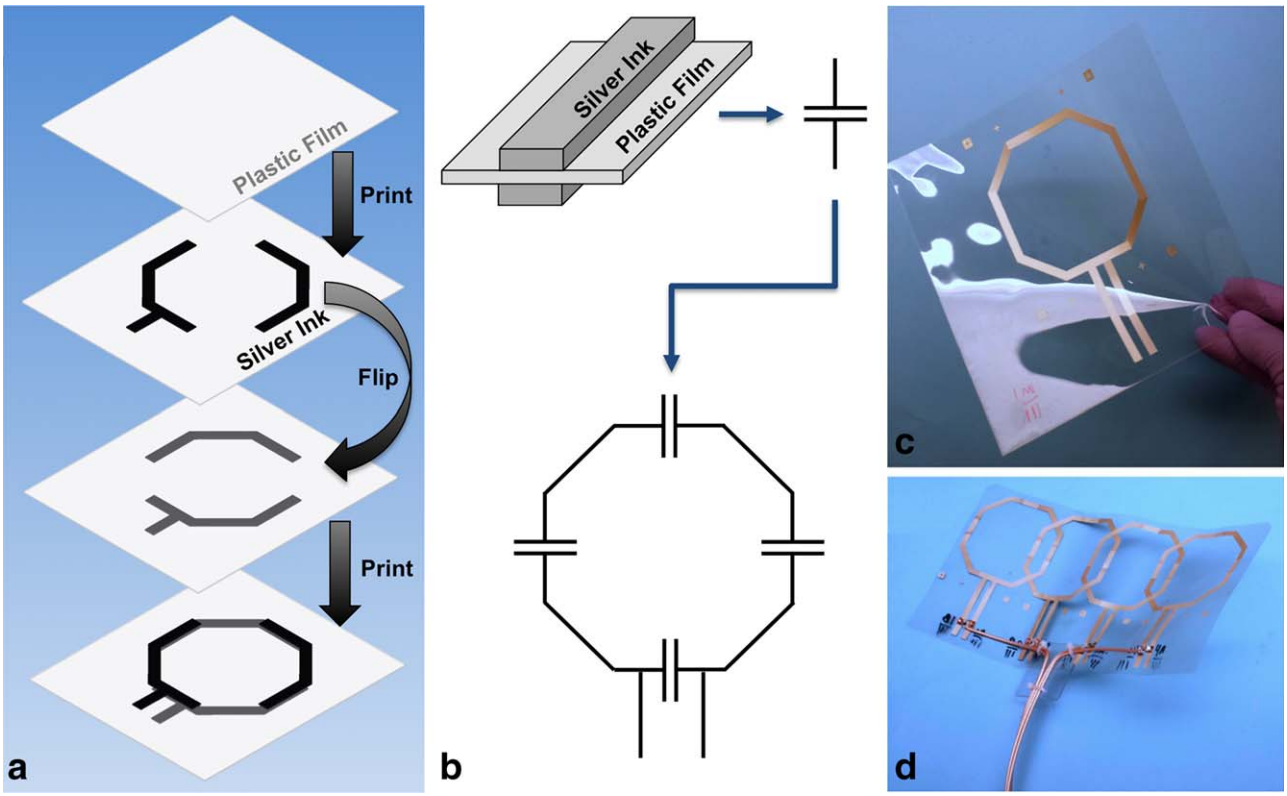

FIG. 1. (**A**) Illustration of the printed coils fabrication process. Conductive features are printed on each side of the substrate to form tuning and matching capacitors. (**B**) Cross-section schematic of coil capacitors formed between two printed metal features and the plastic substrate along with the equivalent circuit of the printed portion of our receive coil. (**C**) Photograph of a single element printed flexible coil. (**D**) Photograph of coil array fabricated using the process flow illustrated in panel A. Single coil elements are shifted to adjacent positions to form a multichannel array. Transmission lines connecting the coils to the MRI scanner are also shown coming out of the bottom of the coil array.

used in the coils, potentially impeding SNR. Although these previous results have been promising, image SNR from printed coils still lags behind conventional coils when compared head-to-head, and the quality of the materials—in particular the capacitor's dielectric—has been identified as an area of possible improvements (11).

In this study, we developed 8.75-cm-diameter octagonal printed coils with $Q_{Unloaded}$ as high as 100 and SNR at 3T as high as 97% of the SNR that a traditional coil displays on a representative phantom. This was achieved by using a coil design wherein the substrate also acted as the capacitor's dielectric and by careful selection of low-loss plastic substrate material. To this end, an experimental apparatus was created to mimic the printed coil geometry by using copper foil for the traces. This apparatus allowed rapid characterization of the dielectric properties of plastic substrates, such that several substrates could be screened rapidly in order to identify the most suitable dielectric for printed coils. The influence of the printed silver trace properties on the $Q_{Unloaded}$ of coils was also investigated. To guide the optimization of the printed coils, we developed an experimental procedure that related a coil's $Q_{Unloaded}$ to its SNR in images of a representative phantom. In particular, this method provided insight into scenarios wherein improvements in $Q_{Unloaded}$ would no longer yield a significant increase in image SNR. Finally, optimized coils were assembled into an eight-channel array for a 3T scanner. The SNR and noise correlation of this array were characterized on a conductive phantom, and its performance was demonstrated by scanning the head of a volunteer. These results were compared with a commercial 12-channel array (3T Head Matrix A Tim Coil; Siemens, Erlangen, Germany). Both arrays produced images of good quality, the printed array displaying an SNR that was six-fold higher near the surface of the phantom near the array elements. At the center of the sample, phantom and human, the SNR of the printed array was half of the conventional array. The signal difference at the center of the phantom was primarily a result of the differences in the overall size and configuration of the arrays, rather than the materials used, showing how printing can be implemented to build high-quality arrays.

METHODS

Fabrication

Coils using a plastic substrate as the dielectric were fabricated by printing the metal features on each side of the substrate (Fig. 1A). The coils were 8.75 cm in diameter with a trace width of 5 mm (see Supporting Fig. S1A for additional details). The metal traces sandwich the substrate, forming integrated tuning and matching capacitors where they overlap (Fig. 1B) (11,14). The area of overlap

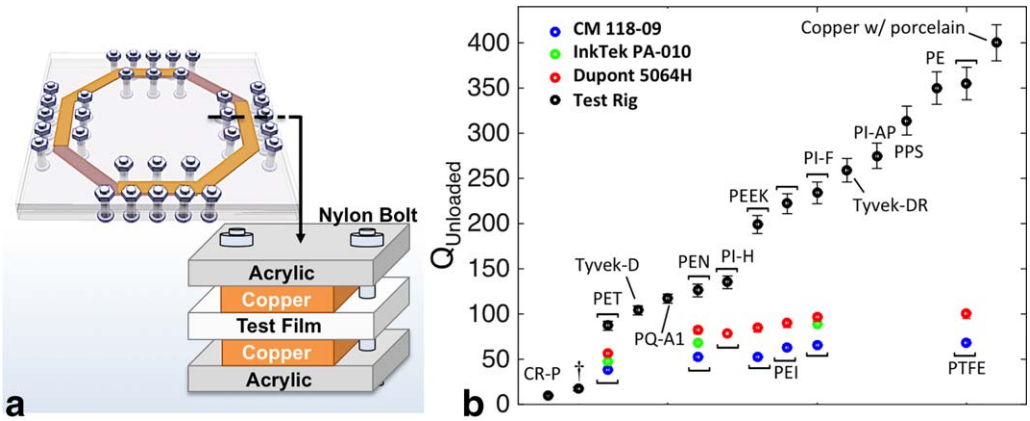

FIG. 2. (**A**) Illustration of the testing rig developed to characterize the dielectric loss of flexible substrates prior to printing. This setup mimics the geometry of the printed coils. The stack of materials is highlighted in the lower right. (**B**) Summary of $Q_{Unloaded}$ of coils obtained with flexible substrate from the testing rig and printed conductive inks. Black points are results from testing rig with copper traces. Blue, green, and red points are from coils printed with CM 118-09, PA-010 and Dupont 5046H respectively. † Denotes the use of the dielectric ink from previous work (10). PTFE is identified as the dielectric with the lowest loss, as it has a highest $Q_{Unloaded}$ in the testing rig at 355 while PET shows the lowest at 87.

between the two plates of the capacitors, as well as the substrate's material and thickness, determined the resulting capacitance. Adding or removing ink on each side of the substrate controlled the capacitor area, and in turn, tuned the coil. A photograph of a printed coil made in this way is shown in Fig. 1C. The total thickness of the coil was 125 μm, contributing to the overall flexibility of the device. Multichannel coil arrays could be fabricated by shifting the single coil pattern during the printing process to an adjacent position on the substrate, as shown in the photograph of a printed four-channel flexible array in Fig. 1D. The critical overlap distance was determined by connecting two tuned printed coils to a network analyzer and measuring what overlap minimized their |S12| interaction (1,15,16). The overlap between each single coil element in the array was 11.7 mm, which resulted in approximately 29 cm of lateral coverage for a four-channel array.

Dielectric Substrates

In the coil configuration used in the present study, the loss characteristics of the plastic substrate had a direct impact on the quality of the printed capacitors, and in turn, image SNR. Dielectric loss was reported for most plastic substrates at limited standard frequencies, but rarely at frequencies common to clinical MRI (i.e., 64, 123.3, and 127.7 MHz). To characterize the dielectric properties of several materials, flat plastic substrates were clamped between two 7-mm-thick acrylic plates with 70-μm-thick copper traces (resistivity $= 1.68 \times 10^{-6}$ Ω-cm) in the same geometry as our coil (Fig. 2A). Acrylic was chosen for the plates for its ease of manufacturing, isotropic electrical properties, ability to withstand clamping forces, and transparency to aid in positioning of the coils, although other low dielectric constant mechanically stable materials could be used.

For each substrate tested, the lengths of the metal traces were adjusted to obtain coil resonance at 123.3 MHz. To measure $Q_{Unloaded}$, the coils were placed at least 50 cm away from any conductive material and the |S12| response from two lightly coupled probes was recorded (7). Probes were decoupled by separating them several diameters apart to reduce baseline |S12| response below −70 dB. Light coupling to the coil under test was ensured by keeping any |S11| or |S22| response above 100 mdB. The Q was measured on a calibrated network analyzer (E5061B ENA; Agilent, Santa Clara, California, USA) with 1601 points averaged 16 times, centered at the Larmor frequency (123.3 MHz) with the vector network analyzer set to a frequency span of 25 MHz. It is important to note that the Q measured on a network analyzer in this way is dependent on the position, orientation, calibration, frequency sweep/span, and day-to-day variation of the experimental setup and is difficult to control for humidity- and temperature-dependent film parameters. Our experimental setup was characterized to have a repeatability of 5% by measuring our control coil several times on different days.

The characterized plastic substrates were selected based on their compatibility with the printing process. The substrates studied are commercially available in a thickness between 50 and 150 μm, are able to withstand at least 125 °C during annealing, and are mechanically stable enough to be handled during processing. The plastic substrates tested were polyethylene, polyethylene terephthalate (PET), polyethylene-napthalate, polyethylene-napthalate with an adhesion layer, kapton 100HN, kapton 200FN919 (PI-F), polyphenylene sulfide, polyetherimide (PEI), polyether ether ketone (PEEK), polytetrafluoroethylene (PTFE), cleanroom paper cellulose with acrylic binder (CR-P), tyvek 1025D (Tyvek D), tyvek brillion 4173DR (Tyvek DR), and pyralux AP.

It should be noted that the acrylic plates of the testing rig contributed a small amount to the overall coil capacitance, because their dielectric constant is higher than air. To characterize this interaction, completed coils with a printed conductor were clamped in the test rig without the copper film to measure any shift in resonance frequency or Q. Resonance frequency shifted down 1.4

MHz on average, implying an increase of ~0.25 pF from the testing rig. Q with and without the acrylic plates changed less than 0.3%, suggesting that any contribution from the acrylic plates was negligible.

Conductive Inks

Three different silver-based conductive inks were compared: Micro-flake Creative Materials 118-09, nanoparticle InkTek PA-010, and micro-flake DuPont 5064H (with resistivity of 7.99×10^{-5} Ω-cm, 3.94×10^{-5} Ω-cm, and 1.84×10^{-5} Ω-cm, respectively, as measured by a four-point probe). Before printing, the substrates were preheated to 140 °C for 10 minutes and cooled again at room temperature to relieve any stress and prevent distortion in future processing steps. Next, the conductive inks were screen printed (ASYS Group ASP01M, Dornstadt, Germany) through a 400 mesh-count stainless steel mesh onto the flexible substrate and annealed at 140 °C for 15 min. This procedure was repeated on the reverse side of the flexible substrates, completing the coils. Printing multiple layers also allowed variation of the thickness of the conductive trace, with each layer adding 5 μm to the printed conductor.

Coils with conductive trace thicknesses of 5–35 μm were examined to characterize the relationship between conductive film thickness, coil $Q_{Unloaded,}$ and mechanical stability. Conductive trace thickness was measured using a stylus profilometer (Dektak 6M Stylus Profilometer; Veeco, Oyster Bay, New York, USA). This characterization was performed with the highest conductivity ink (DuPont 5064H) on low-loss (PTFE) and higher-loss (PET) substrates to show the relative benefits of conductive ink optimization.

Coils were made for SNR measurements by printing DuPont 5064H silver ink on several types of substrates. During tuning, the coil's resonance frequency and input impedance were monitored with the same vector network analyzer as described previously. The coils are tuned to the Larmor frequency of protons of our 3T scanner (123.3 MHz; 3T Siemens TIM Trio) and an input impedance of 50 Ω when loaded (6).

Imaging

To serve as reference, control coils were fabricated by soldering high-quality ATC capacitors on 35-μm-thick copper traces on Pyralux AP substrates. The geometry of the control coil was identical to the printed ones. To predict the SNR of printed coils without scanning, Q_{Loaded} was measured and compared with that of a control coil. To load the coils, they were placed directly on top of a water-filled 7L cubic phantom doped with 3.356 g/L $NiCl_2{\cdot}6H_20$ and 2.4 g/L NaCl for conductivity of 0.68 S/m at 123 MHz. The acrylic walls of the phantom were 6.4 mm thick.

To obtain a direct measurement of SNR, the coils were used to image the conductive phantom on a 3T scanner (3T Siemens TIM Trio). A 2D gradient echo sequence with an echo time of 10 ms, pulse repetition time of 438 ms, flip angle of 25 °, and slice thickness of 5 mm was used to scan. The field of view was $200 \times 200\,mm^2$ with a resolution of 256 phase encodes and readouts. Printed portions of the coil were clamped into a test board that contained a PIN diode to deactivate the coil during the transmit phase of each scan (Supporting Fig. S1B). This board was connected to a gateway box (Stark Contrast, Erlangen, Germany) containing preamplifiers via a half-wavelength-long coaxial RG-316 cable. Several cable traps were placed on the half-wavelength coaxial cable to reduce coupling of the cable to the scanner's body transmit coil. The SNR of images was measured by dividing the average signal (i.e., the average magnitude from a 4×18 cm region of pixels along the entire length of the phantom) by an estimate of the noise standard deviation. Pixels near the center of the coil were chosen to measure the signal to avoid clipping artifacts from saturated regions near the edges of the coil where the conductor traces were. Image analysis was performed on raw data files from the scanner rather than exported images to avoid compression and signal clipping artifacts. The noise was calculated from an area with no signal containing at least 2800 points at least 5 pixels from the edge of the image with no streaking artifacts. All SNR measurements were normalized to images taken with the traditionally made high-quality ($Q_{Unloaded} = 400$) coils. To show the benefit of using the substrate as the dielectric compared with printing dielectric inks, a coil was fabricated using the same Creative Materials 116-20 dielectric ink as reported previously (11).

Coil Array

An eight-channel printed array was fabricated from printed elements and compared with a 12-channel commercially available coil (Siemens 3T Head Matrix A Tim Coil). The commercial array had elements approximately 25 cm long and 8 cm wide in a single row surrounding the enclosed cylindrical volume.

To simplify processing, and to be consistent with the single coil experiments, the same printed coil dimensions used for single coil characterization were kept. The entire printed coil array was laminated in 125 μm of PTFE plastic to prevent skin contact, provide flame resistance, and maintain high breakdown strength for any DC bias that could exist on the coil. The printed array connected to the scanner in the same manner as single coil elements except for the interface between printed and nonprinted portions. The printed films were cut to expose conductive leads that are folded over sections of RG-316 and copper braid, locked into place using a brass ring crimp (a detailed photograph is available in Supporting Fig. S1C). The entire crimped junction was then laminated in PTFE with the rest of the coil. Each of the two gateways accepted four channels, providing eight channels in total. The commercial array used the built-in commercial preamplifiers and connectors that can accommodate additional channels. Images were taken of a 3.8 L cylindrical loading phantom doped with 4.5 g/L NaCl and 2.9 g/L of $NiCl_2{\cdot}6H_20$. The coils were placed directly onto the phantom that had a 6-mm-thick acrylic wall containing the solution. SNR maps were obtained by first computing the noise covariance matrices from noise images obtained using no radiofrequency (RF) power or gradients, which were used in a Roemer

optimal combination (i.e., SENSE with no acceleration factor) (1,17). For this analysis, coil sensitivity maps were estimated with ESPIRiT (18). The noise correlation coefficient matrices were also calculated from noise images obtained using no RF power or gradients and computed using Equation 1 in Duensing et al. (19).

Volunteer Imaging

To scan a volunteer, a 3D ultrafast gradient echo sequence was used with 1.1-mm cubic voxels. The pulse repetition time and echo time were 1900 ms and 2.51 ms, respectively. A 9° flip angle was used with 246 phase and frequency encodes and no averaging. The eight-channel array was wrapped around the head of the volunteer with a 3-mm foam mat placed between the coil and the skin to reduce capacitive coupling. Human experiments were performed with approval of the Internal Review Board at the University of California, Berkeley.

Predicting SNR

An experimental method was developed to relate the $Q_{Unloaded}$ of a coil with its SNR in an image of a homogeneous phantom with similar conductivity to human tissue to simplify testing procedures.

If the $Q_{Unloaded}$ and Q_{Loaded} on a particular phantom were known, the efficiency of a coil was predicted using Equation 5.35 from Link in Rudin (20), shown here in Equation 1 where SNR_0 is the total available (i.e., intrinsic) SNR (21,22):

$$SNR = SNR_0\sqrt{1 - \frac{Q_{Loaded}}{Q_{Unloaded}}} \quad [1]$$

However, when evaluating materials, particularly if they are in a nonconforming test rig as described here, it is difficult to place it in close contact with phantoms, especially if a curved phantom is desired. Although it is possible to measure both $Q_{Unloaded}$ and an approximate Q_{Loaded} with a coil made with the test rig, it is more convenient to only measure $Q_{Unloaded}$. To do this, an alternate means of coil comparison is needed.

The Q_{Loaded} of a coil-sample system is related to the total loss of the system, with contributions from the coil materials (R_{Coil}), and the sample (R_{Sample}). $Q_{Unloaded}$ is only influenced by R_{Coil}. Equations 2 and 3, taken from Equations 5.30 and 5.31 from Link in Rudin (20), describe this relationship where L is the inductance of the coil, and ω is the resonance frequency (7,8,23).

$$Q_{Loaded} = \frac{\omega L}{R_{Coil} + R_{Sample}} \propto \frac{1}{R_{Coil} + R_{Sample}} \quad [2]$$

$$Q_{Unloaded} = \frac{\omega L}{R_{Coil}} \propto \frac{1}{R_{Coil}} \quad [3]$$

The SNR of an image obtained from a coil can then be related to its Q_{Loaded}, as described by Equation 5.33 from Link in Rudin et al. (7,17,20,24):

$$SNR \propto \sqrt{Q_{Loaded}} \quad [4]$$

There are a multitude of factors that impact image SNR and play into the coefficient of proportionality implied in Equation 4. To determine a coil's performance without having to estimate this coefficient, one strategy is to compare it with a geometrically identical coil known to have low-loss (i.e., a coil that has an efficiency of approximately 99% or greater). If two coils have the same geometry and are in the same position, then L and R_{Sample} are not significantly changed. Making this assumption, it is then possible to predict the relative SNR in images obtained from a test coil with the SNR obtained from a high-quality control coil, as shown Equation 5:

$$Relative\,SNR(\%) = \frac{\sqrt{Q_{LoadedTest}}}{\sqrt{Q_{LoadedControl}}} \quad [5]$$

The Q_{Loaded} of a coil can be estimated from its $Q_{Unloaded}$ with Equation 6:

$$Q_{Loaded} \propto \left(\frac{1}{Q_{Unloaded}} + R_{Sample}\right)^{-1} \quad [6]$$

Measurements of $Q_{Unloaded}$, Q_{Loaded}, and SNR of several completed coils allowed estimation of the sample loss factor, R_{Sample}, used to represent the loss contribution from the 7L 0.68 S/m water-based phantom. Finally, by combining Equations 5 and 6, the relative SNR of a test coil to that of a control coil can be estimated simply from the measurement of its $Q_{Unloaded}$.

$$Relative\,SNR(\%) = \sqrt{\frac{(Q_{UnloadedControl})^{-1} + R_{Sample}}{(Q_{UnloadedTest})^{-1} + R_{Sample}}} \quad [7]$$

RESULTS

Ink and Substrates Characterization

Figure 2B compares the $Q_{Unloaded}$ of all substrates tested in the copper/acrylic testing rig as well as the $Q_{Unloaded}$ of some printed coils made from the same substrates with the three silver inks (the results are tabulated in Supporting Table S1). The $Q_{Unloaded}$ in the testing rig ranged from 10 for CR-P to 355 with PTFE, which is very close to the $Q_{Unloaded}$ of control coils made with high-quality porcelain capacitors. However, for printed coils, the $Q_{Unloaded}$ for all three silver inks did not reach values higher than 100, despite using substrates that achieved high $Q_{Unloaded}$ in the copper test rig. For example, the PTFE film had the highest $Q_{Unloaded}$ in the copper test rig, but when a printed conductor was used, the $Q_{Unloaded}$ was 100, which was not significantly higher than a printed coil made with PI-F, PEI, or PEEK.

As the thickness of the silver ink was increased from 5 to 35 μm on PET and PEEK substrates (Fig. 3A), a diminishing return in coil $Q_{Unloaded}$ was observed above 20 μm of ink (Fig. 3B). Furthermore, it was seen that the silver thickness had a more dramatic influence on $Q_{Unloaded}$ with the PTFE substrate than PET due to the higher dielectric loss of PET.

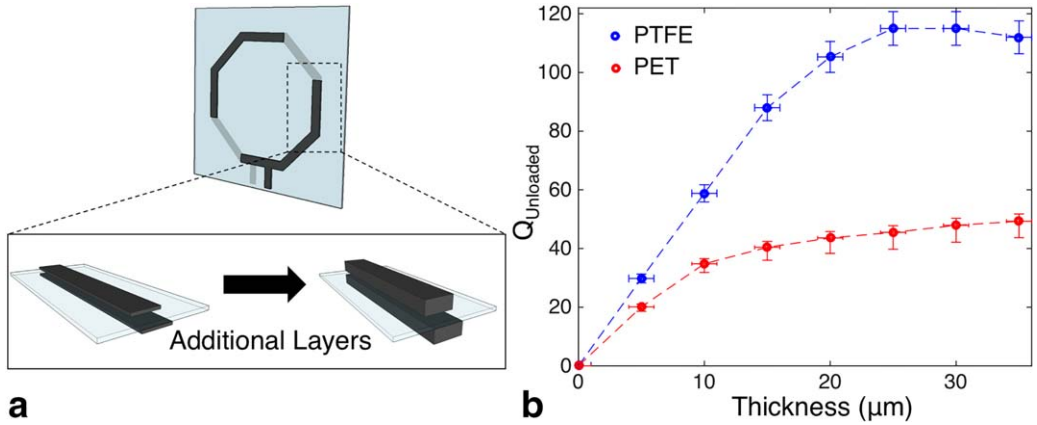

FIG. 3. (**A**) Illustration of a printed coil with inset showing an increase of the printed layer (gray) thickness, obtained by printing additional layers of conductor. (**B**) $Q_{Unloaded}$ of coils made with increasing thickness of DuPont 5064H silver ink for highest (PTFE) and lowest (PET) performing flexible substrates in blue and red.

Image SNR

The SNR extracted from images from printed coils on a conductive phantom (Fig. 4A) are summarized in Fig. 4B. Figure 4B shows that all coils improve significantly over the printed coil previously reported with a solution processed dielectric (11). Furthermore, all coils are within 8% of SNR of the high-quality control coil. The diminishing effect a coil's $Q_{Unloaded}$ has on SNR in the conductive phantom images is illustrated in Fig. 4C, where $Q_{Unloaded}$ of printed coils is plotted against SNR relative to the control coil (tabulated in Supporting Table S2). The results from our model are also shown in Fig. 4C with the sample fitting parameter, R_{Sample}, equal to 0.087 ($R^2 = 0.97$). The values obtained from our predictions are in close agreement with the value predicted from Link in Rudin (20).

Printed Array

To clearly compare the SNR between conventional and printed coil arrays, both arrays were first used to image a homogeneous conductive phantom, as shown in Fig. 5A. The SNR maps shown in Fig. 5B illustrate that the SNR for the printed coil was highest at the surface of the phantom. This was especially true for regions near the conductive traces of each element, which yielded a printed array with an SNR six times higher than that obtained with the commercially available array. However, near the center of the phantom, the printed array produced 49% of the SNR compared with the commercial array.

The noise correlation coefficients for each array were characterized by noise images obtained from scans with no RF excitation. Figure 5C shows the noise correlation coefficients for both the printed and the control array, with an average correlation coefficient of 0.105 for the printed array and 0.041 for the control array. The coil overlap coupling capacitance was 21.4 pF. The isolation ($|S_{12}|$) between adjacent coil elements was 17.2 ± 2.7 dB with a nonadjacent next nearest neighbor value of 20.4 ± 2.3 dB.

Finally, the eight-channel printed array was wrapped around the head of a volunteer (Fig. 6A). Figure 6B shows brain images taken with the printed eight-channel

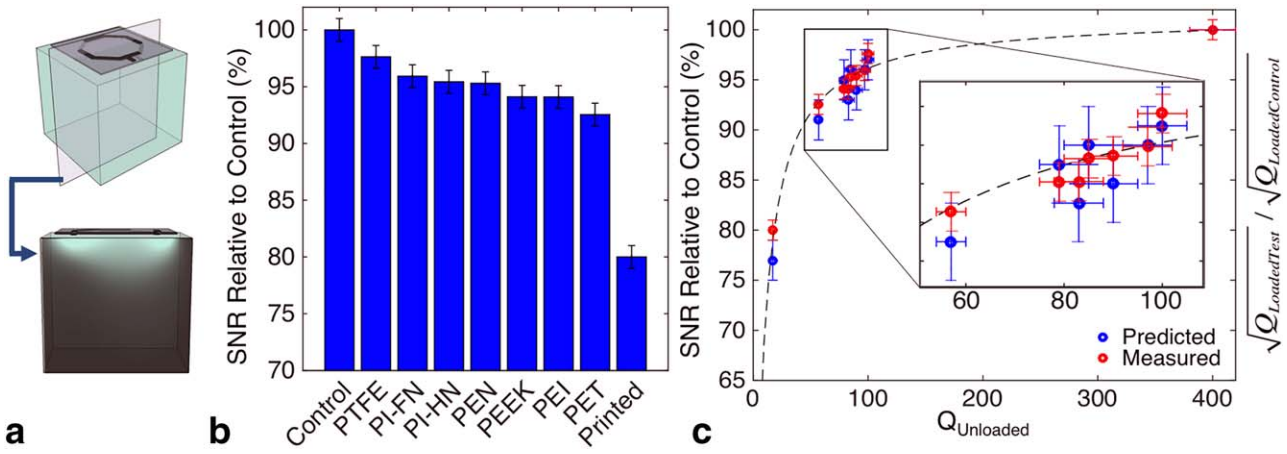

FIG. 4. (**A**) Illustration showing a coil on a 7-L conductive phantom for measurements of Q_{Loaded} and image SNR. A slice of the phantom is highlighted with an overlay of a scan showing the sensitivity profile for printed coils at 3T. (**B**) Relative SNR of printed coils made with several substrates and Dupont 5064H silver ink loaded with a conductive phantom and measured at 3T as a percentage of the control. Measurements were taken at center of the coils along the length of the phantom. (**C**) SNR relative to control versus $Q_{Unloaded}$ for all coils as predicted from bench top measurements (blue) and on a 3T scanner (red). The black dotted trend line indicates the fit of the data using the model.

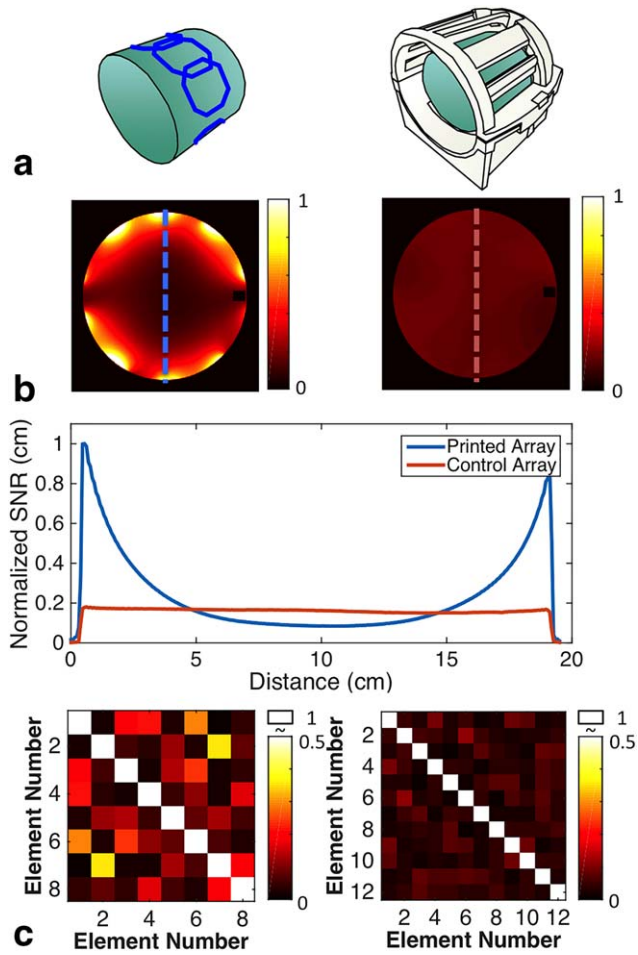

FIG. 5. (**A**) Illustration of a cylindrical conductive phantom (green) showing the placement of (left) an eight-channel printed array and (right) a commercially available 12-channel head array. (**B**) SNR maps of the phantom using (left) the printed coil array and (right) the commercial array. Blue and red dotted lines highlight the location of SNR cross sections shown in the plot below. SNR was normalized to the maximum SNR seen with the printed array. The printed array showed higher SNR near the surface and slightly lower SNR in the center compared with the commercial array due to different element geometry and layout. (**C**) Noise correlation coefficient matrix for (left) the printed array and (right) the commercial array from images without RF excitation. The average off-diagonal coefficient for the printed matrix was 0.105 (min: 0.007 and max: 0.357), whereas that for the commercial array was 0.041 (min: 0.002 and max: 0.113).

array and the 12-channel commercial array. Images produced from each array were similar in quality, with SNR trends similar to the ones shown on the phantom in Fig. 5B.

DISCUSSION

Although previous studies have shown the feasibility of imaging animals (12) and humans (11) with printed coils, further understanding of the materials available to an array designer can increase performance. Printing receive coils for clinical imaging is unique because the primary noise in the system usually comes from the sample, not the coil itself (8). Identifying cases in which increasing coil quality will have diminishing impact can allow an array designer to add functionality by choosing a different material set.

Ink and Substrates Characterization

The testing apparatus allowed the characterization of $Q_{Unloaded}$ for coils made using several plastic substrates as dielectric material in coil capacitors. Because copper foil was used for the conductive part of the loop, it can be assumed that the coil losses were dominated by the dielectric losses, and therefore $Q_{Unloaded}$ was an indirect measurement of the dielectric quality of each tested material. The gap seen in $Q_{Unloaded}$ between the printed and test rig coils in Fig. 2B indicates that, for most substrates, the $Q_{Unloaded}$ of printed coils was limited by the conductivity of the printed conductors. However, on the substrates that displayed the most loss, such as PET, changing the silver ink only raised $Q_{Unloaded}$ from 38 to 57, indicating that the low values of $Q_{Unloaded}$ stemmed from losses of both the substrate and the conductive ink. Overall, these results indicate the potential of plastic substrates to be used as dielectrics in very high $Q_{Unloaded}$ coils. However, when printed conductors were used, they tended to limit the maximum values attainable for $Q_{Unloaded}$. As a result, other substrate properties, such as mechanical or thermal stability, could be taken into account to select the best suitable substrate for a particular application of printed coils. Reducing the losses generated by the printed conductors represents a major avenue for improving the $Q_{Unloaded}$ of printed coils.

One method to boost the conductivity of printed silver traces, and in turn coil $Q_{Unloaded}$, is to increase the trace thickness, as illustrated in Fig. 3A. As shown in Fig. 3B, very thick films of printed conductor did not drastically improve $Q_{Unloaded}$ because of the diminishing contribution on the trace's cross sectional area, and because the skin effect limits the effective thickness of material which contributes to charge conduction. A slight decrease in $Q_{Unloaded}$ was even seen for very thick conductive silver films on PTFE, most likely due to the occurrence of the film cracking and thus reducing conductivity. Based on those observations, a thickness of 15 μm of silver printed from the DuPont 5064H ink was chosen as the optimal fabrication parameter for subsequent coils to maintain sufficient SNR while avoiding film cracking.

Image SNR

All coils made with flexible substrates showed higher $Q_{Unloaded}$ and image SNR than the fully printed dielectric coils described in the previous study. This difference was attributed to the low loss the substrates display and to the higher loss in binders present in most types of printable dielectric ink.

The results shown in Fig. 4C of the single printed coil testing, along with the trend from our model, suggest that coils with a $Q_{Unloaded}$ of 100 or more would only see a marginal increase (~3%) in SNR compared with the control. Even a printed coil made of PET, which had a $Q_{Unloaded}$ of 58, displayed 92% of the SNR of the control coil. To put these findings in perspective, a 3%–

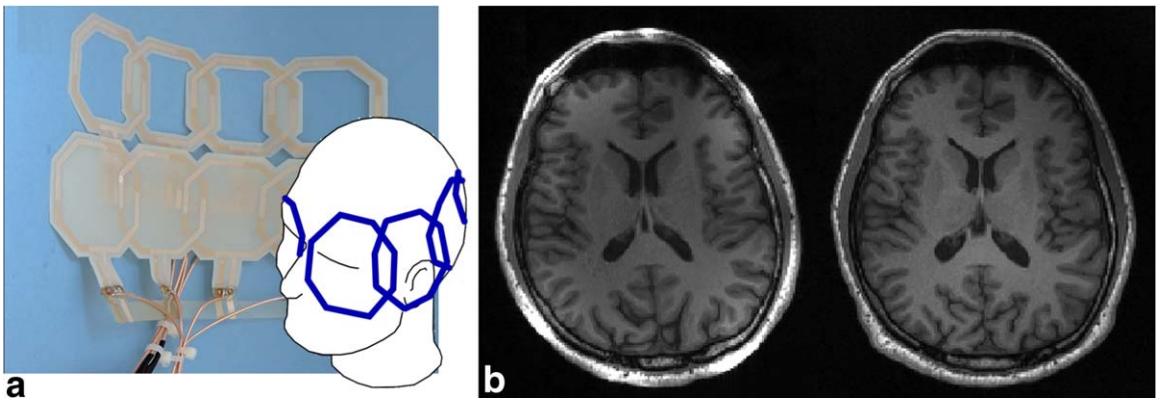

FIG. 6. (**A**) Photograph of two printed four-channel arrays combined to make an eight-channel array. Placement on a volunteer is shown in the bottom right-hand corner. (**B**) Axial slice of a volunteers' brain using (left) the printed coil array and (right) the commercially available 12-channel head array. Similar to phantom images, the printed coil showed higher SNR near the surface of the brain and slightly lower SNR in the center of the brain compared with the commercial 12-channel array.

8% decrease in SNR is roughly equivalent to a coil being offset from the body by only 1–1.8 cm (11). In a worst-case nonclinical scenario wherein the imaged sample would be nonconductive (and thus nonloading), the PTFE coil with a $Q_{Unloaded}$ of 100 would still show 50% of the SNR of the control coil. Therefore, even with improvements in the properties of printed materials, only marginal improvements in SNR can be expected. However, the high flexibility of printed coils may provide patients with more comfort while consistently delivering images with high SNR.

Printed Array

From our proof-of-concept printed eight-channel array fabricated using DuPont 5064H and a PEEK substrate, we were able to produce SNR and noise correlation numbers comparable to a commercially available 12-channel array. Other substrates such as PTFE, PEI, and PI-F showed better coil performance but lacked mechanical and environmental stability, preventing their use in arrays that are suitable and safe for human imaging without additional steps. Specifically, PTFE had poor film adhesion, causing cracking to occur at any printed/non-printed interface that existed between the coil substrate and the cables used for connection, whereas PEI and PI-F absorbed enough moisture from the air to significantly change tuning over time.

The close proximity to the sample and the smaller element size of the printed array yielded higher SNR at the surface but did not yield as much penetration as the 12-channel commercial array, achieving only 49% of the SNR at the center of the phantom. The differences in the SNR maps for the printed and control coils were most likely due to the differences in the surface areas between the arrays, positioning, layout, and preamplifier noise figure.

Although the printed array showed higher noise correlation than the control array, our results are comparable to the literature regarding 3T surface coil arrays (25–27). The higher correlation coefficient is attributed to the close proximity to the sample in addition to the relatively large mutual capacitance between channels. We have identified other pathways for improvement of printed arrays, such as better cable management, optimized coil placement, and additional input baluns. Such optimizations would produce lower noise correlation numbers, but are beyond the scope of the work presented here.

The image quality is similar with both coil arrays, despite the vast difference in component quality and number of channels. Although this is not a rigorous comparison between the two coil sets (e.g., coil shape, layout, and connection to the scanner affect overall performance), it nonetheless illustrates how close the performance of printed coils can be to conventional, commercial systems.

CONCLUSION

As materials and methods for printing continue to improve, the characterization techniques described here can serve as practical tools to enable quick identification of highly performing flexible substrates and conductors for printing MRI receive coil arrays. In this study, we demonstrate a printed coil with an SNR within 3% of a conventionally fabricated control coil. The tests performed highlight the importance of optimizing materials used in printed coils. Using this approach, we have shown that receive coil arrays fabricated using printing techniques are comparable to commercially available arrays, while offering new form factors and lightweight construction.

ACKNOWLEDGEMENTS

We thank Anita Flynn, Thomas Grafendorfer, James Tropp, Victor Taracila, and Fraser Robb, along with GE Healthcare, for guidance with electrical testing of coils.

REFERENCES

1. Roemer PB, Edelstein WA, Hayes CE, Souza SP, Mueller OM. The NMR phased array. Magn Reson Med 1990;16:192–225.
2. Wright SM. Full-wave analysis of planar radiofrequency coils and coil arrays with assumed current distribution. Concept Magnetic Res 2002;15:2–14.
3. Jin J-M. Electromagnetic analysis and design in magnetic resonance imaging. Boca Raton, FL: CRC Press; 1998. 282 p.

4. Nishimura DG. Principles of magnetic resonance imaging. Stanford, CA: Stanford University; 2010. 238 p.
5. Lauterbur PC. Image formation by induced local interactions: examples employing nuclear magnetic resonance. Nature 1973;242:190–191.
6. Mispelter Jl, Lupu M, Briguet A. NMR probeheads for biophysical and biomedical experiments: theoretical principles and practical guidelines. London: Imperial College Press; 2006. 756 p.
7. Hayes CE, Axel L. Noise performance of surface coils for magnetic-resonance imaging at 1.5-T. Med Phys 1985;12:604–607.
8. Darrasse L, Ginefri JC. Perspectives with cryogenic RF probes in biomedical MRI. Biochimie 2003;85:915–937.
9. Doty FD. Solid state NMR probe design. In: Encyclopedia of Magnetic Resonance. Hoboken, NJ: John Wiley & Sons; 2007.
10. Krebs FC. Fabrication and processing of polymer solar cells: a review of printing and coating techniques. Solar Energy Materials and Solar Cells 2009;93:394–412.
11. Corea JR, Flynn AM, Lechene B, Scott G, Reed GD, Shin PJ, Lustig M, Arias AC. Screen-printed flexible MRI receive coils. Nat Commun 2016;7:10839.
12. Mager D, Peter A, Tin LD, Fischer E, Smith PJ, Hennig J, Korvink JG. An MRI receiver coil produced by inkjet printing directly on to a flexible substrate. IEEE Trans Med Imaging 2010;29:482–487.
13. Horch RA, Gore JC. 3D-Printed RF Coils for Solution-State NMR: Towards Low-Cost, High-Throughput Arrays. In Proceedings of the 23rd Annual Meeting of ISMRM, Toronto, Ontario, Canada, 2015.
14. Sadiku MNO. Elements of electromagnetics. New York: Oxford University Press; 2011. Abstract number 0853. 820 p.
15. Wright SM, Wald LL. Theory and application of array coils in MR spectroscopy. NMR Biomed 1997;10:394–410.
16. Keil B, Wald LL. Massively parallel MRI detector arrays. J Magn Reson 2013;229:75–89.
17. Pruessmann KP, Weiger M, Scheidegger MB, Boesiger P. SENSE: sensitivity encoding for fast MRI. Magn Reson Med 1999;42:952–962.
18. Uecker M, Lai P, Murphy MJ, Virtue P, Elad M, Pauly JM, Vasanawala SS, Lustig M. ESPIRiT—an eigenvalue approach to autocalibrating parallel MRI: where SENSE meets GRAPPA. Magn Reson Med 2014;71:990–1001.
19. Duensing GR, Brooker HR, Fitzsimmons JR. Maximizing signal-to-noise ratio in the presence of coil coupling. J Magn Reson B 1996; 111:230–235.
20. Rudin M. In-vivo magnetic resonance spectroscopy I: probeheads and radiofrequency pulses spectrum analysis (NMR basic principles and progress). Berlin, Heidelberg: Springer Berlin Heidelberg; 1992. 284 p.
21. Edelstein WA, Glover GH, Hardy CJ, Redington RW. The intrinsic signal-to-noise ratio in NMR imaging. Magn Reson Med 1986;3:604–618.
22. Mansfield P, Morris PG. NMR imaging in biomedicine. New York: Academic Press; 1982. 354 p.
23. Pozar DM. Microwave engineering. Hoboken, NJ: John Wiley & Sons; 2005. 700 p.
24. Vaughan JT, Griffiths JR. RF coils for MRI. Chichester, West Sussex: John Wiley & Sons; 2012.
25. Keil B, Blau JN, Biber S, Hoecht P, Tountcheva V, Setsompop K, Triantafyllou C, Wald LL. A 64-channel 3T array coil for accelerated brain MRI. Magn Reson Med 2013;70:248–258.
26. Nordmeyer-Massner JA, De Zanche N, Pruessmann KP. Stretchable coil arrays: application to knee imaging under varying flexion angles. Magn Reson Med 2012;67:872–879.
27. Wiggins GC, Triantafyllou C, Potthast A, Reykowski A, Nittka M, Wald LL. 32-channel 3 Tesla receive-only phased-array head coil with soccer-ball element geometry. Magn Reson Med 2006;56:216–223.

SUPPORTING INFORMATION

Additional Supporting Information may be found in the online version of this article

Supporting Figure S1. (**A**) Detailed dimensions of the printed coils. (**B**) Photographs showing the board interfacing between printed and non-printed components for single coil testing. The board contains a nonmagnetic SMA end-launch connector, PIN diode, and discrete inductor for tuning Q spoiling. Nylon bolts are used to clamp through the coil and board. A thin copper strip is soldered onto the board to make top contact to the coil. (**C**) Close-up photograph showing brass ring crimp used to join the printed array to RG-316 cables and copper braid.

Supporting Table S1. $Q_{Unloaded}$ of printed coils and substrates in testing rig. A mark of "-" denotes that the ink was unable to adhere to material. †Printed coils from previous work 11 were tested with a printed conductor, not in the copper and acrylic test rig.

Supporting Table S2. Bench top measurements and scanning results of SNR relative to control coils. Printed coils were fabricated with DuPont 5064H ink.

Supporting Materials for:

Materials and methods for higher performance screen-printed flexible MRI receive coils

Authors: Joseph R. Corea[1], P. Balthazar Lechene[1], Michael Lustig[1], and Ana C. Arias[1*]

Affiliations:
[1]Department of Electrical Engineering and Computer Sciences, University of California, Berkeley, CA 94720, USA.

*Correspondence to: acarias@eecs.berkeley.edu

508 Cory Hall, Berkeley CA, 94720, USA

+1 510-642-1728

Supporting Table S1: $Q_{Unloaded}$ of printed coils and substrates in testing rig. A mark of "-" denotes that the ink was unable to adhere to material. †Printed coils from previous work (11) were tested with a printed conductor, not in the copper and acrylic test rig.

Substrate	Testing rig 1.68e-6 Ω*cm	CM 118-09 7.99e-5 Ω*cm	IT PA-101 3.94e-5 Ω*cm	DP 5064H 1.84e-5 Ω*cm
Copper Coil with ATC Capacitors	400 ± 20	-	-	-
Teflon (PTFE)	355 ± 18	68.7 ± 3	-	100 ± 5
Poly Ethylene (PE)	350 ± 18	-	-	-
Polyphenylene Sulfide (PPS)	314 ± 16	-	-	-
Pyralux AP (PI)	275 ± 14	-	-	-
Tyvek Brillion 4173DR (TyvekDR)	259 ± 13	-	-	-
Kapton 200FN919 (PI-N)	234 ± 12	66 ± 3	89 ± 5	97 ± 5
Ultem Polyetherimide (PEI)	222 ± 11	63 ± 3	-	90 ± 5
Polyetheretherketone (PEEK)	199 ± 10	52 ± 3	-	85 ± 5
Kapton 100HN (PI)	135 ± 7	-	-	79 ± 4
Polyethylene Naphthalate Q65HA (PEN)	126 ± 7	52 ± 3	68 ± 4	83 ± 5
Polyethylene Naphthalate PQ A1 (PQA1)	117 ± 5	-	-	-
Tyvek 1025D (TyvekD)	104 ± 5	-	-	-
Polyethylene Terephthalate (PET)	87 ± 5	38 ± 2	48 ± 3	57 ± 3
Prior Printed Coils(11)	17 ± 2†	-	-	-
Clean Room Paper (CR-P)	10 ± 2	-	-	-

Supporting Table S2: Bench top measurements and scanning results of SNR relative to control coils. Printed coils were fabricated with DuPont 5064H ink.

Substrate	Unloaded Q	Loaded Q	Predicted SNR	Measured SNR
Copper Coil with ATC Capacitors	400 ± 20	10.2 ± 0.3	100.0	100.0 ± 0.3
Teflon (PTFE)	100 ± 5	9.6 ± 0.3	97 ± 2	97 ± 0.7
Kapton 200FN919 (PI-N)	97 ± 5	9.4 ± 0.3	96 ± 2	95.4 ± 1.0
Ultem Polyetherimide (PEI)	90 ± 5	9.1 ± 0.3	94 ± 2	93.2 ± 0.9
Polyetheretherketone (PEEK)	85 ± 5	9.5 ± 0.3	96 ± 2	93.7 ± 0.9
Polyethylene Naphthalate Q65HA (PEN)	83 ± 5	8.9 ± 0.3	93 ± 2	94.8 ± 1.0
Kapton 100HN (PI-N)	79 ± 4	9.2 ± 0.3	95 ± 2	94.9 ± 0.6
Polyethylene Terephthalate (PET)	57 ± 3	8.5 ± 0.3	91 ± 2	91.8 ± 0.5
Prior Printed Coils(11)	17 ± 2	6.0 ± 0.3	77 ± 2	79.6 ± 0.6

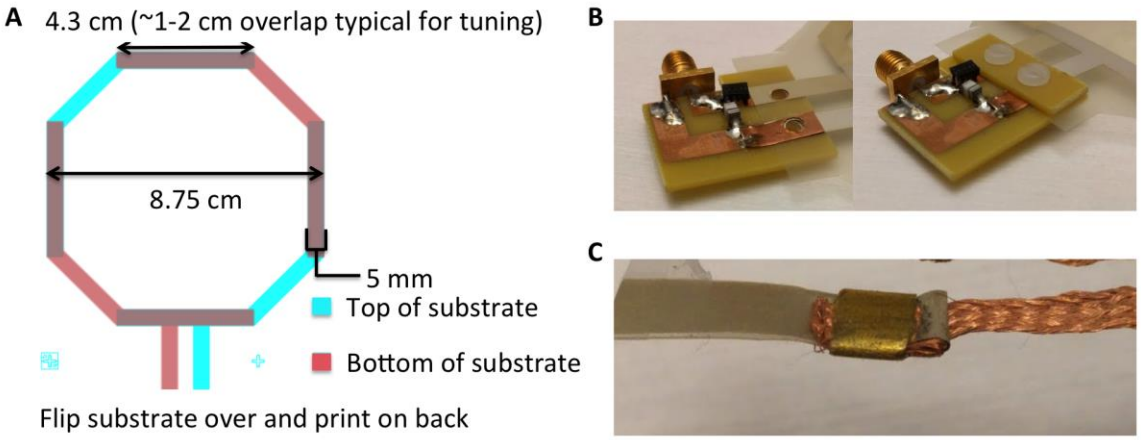

Supporting Fig. S1: A. Detailed dimensions of the printed coils. **B.** Photographs showing the board interfacing between printed and non-printed components for single coil testing. The board contains non-magnetic SMA end-launch connector, PIN diode, and discrete inductor for tuning Q spoiling. Nylon bolts are used to clamp through the coil and board. A thin copper strip is soldered onto the board to make top contact to the coil. **C**. Close up photograph showing brass ring crimp used to join the printed array to RG-316 cables and copper braid.

Incompatible Substrates

Some of the substrates tested, specifically PPS, PE, Tyvek-D, Tyvek-DR, and cleanroom paper, could not be printed on because the 140 °C temperature in the curing step caused significant warping or melting of the substrates. PQ-A1 is a poor candidate for this process because of a Q-lowering adhesion layer that was only on one side of the film, additionally polyimide based Pyralux AP was not available without a copper cladding. Some inks did not adhere well to all the substrates and delaminated preventing a complete coil circuit to be formed (tabulated data in ST1).